

Microstructures and high temperature oxidation resistance of alloys from Nb–Cr–Si system

S. K. Varma · Clemente Parga · Krista Amato · Jennifer Hernandez

Received: 14 January 2010/Accepted: 29 March 2010/Published online: 10 April 2010
© Springer Science+Business Media, LLC 2010

Abstract Oxidation behavior of Nb–30Si–(10,20)Cr alloys have been evaluated in air from 700 to 1400 °C by heating for 24 h and furnace cooling them. The lower weight gain per unit area has been observed for 20Cr alloy at 1200, 1300, and 1400 °C. Pestling has been observed at lower temperatures (700, 800, 900 °C). Analysis indicates that the powder formation at 900, 100, 1100 °C may be associated with β form of Nb_2O_5 (base centered monoclinic form). However the *m*-monoclinic form of Nb_2O_5 evolves at temperatures above 900 °C while *o*-orthorhombic Nb_2O_5 forms at below this temperature. The phases in the alloys have been calculated using the PandatTM software program at different temperatures using calculated Nb–Cr–Si phase diagrams.

Introduction

Nb-based alloys are continuously being explored to develop the high temperature materials, especially for structural purposes. Although these alloys may show adequate mechanical behavior at elevated temperatures, oxidation resistance remains an issue that has not been resolved yet. There are extensive efforts being made to improve the oxidation resistance by the addition of suitable alloying elements.

The present group of researchers is studying the Nb-based alloys for possible application as a high temperature material with special emphasis being placed on the

oxidation resistance at elevated temperatures [1–7]. The effect of alloying additions on the oxidation resistance has been evaluated by Chan [8, 9] and Bewlay et al. [10, 11]. Bewlay et al. [11] indicate the presence of a solid solution phase (α) rich in Nb, 5–3 silicide (Nb_5Si_3), and Laves phase (NbCr_2) in Nb–8Cr–16Si and Nb–25Cr–12Si alloys. The eutectic like microconstituent consists of these three phases. It appears that various compositions of the alloys from Nb–Cr–Si system contain similar microstructures. Obviously, NbCr_2 phase has been considered as very desirable for enhancing the oxidation resistance [1, 5, 7] while α phase is not beneficial for such purposes. Recently [12], addition of Al to the Laves phase has shown to improve the oxidation resistance at 1373 and 1473 K. Alloyed Laves phase was tested up to 12 at.% Al.

Niobium silicides in the form of refractory metal intermetallic composites (RMIC) may be another promising family of materials for use in aircraft-engine performance enhancement [13]. RMICs contain niobium silicides with high strengths while Nb-based solid solution may provide the necessary toughness. Alloying additions with Ti, Hf, Cr, and Al can provide a highly desirable set of properties for high temperature creep strengths, oxidation resistance, and even room temperature toughness [14].

One of the major problems encountered in Nb-based alloys for oxidation purposes is pesting and spallation. Relative rapidity with which certain alloying elements oxidize and the differences in the coefficient of thermal expansion values of the oxides in the scale may be the contributing factors [15]. The phenomena, however, have been usually observed, in general, in a range of temperature from 800 to 1100 °C depending on the alloying elements [1].

Oxidation studies conducted on Ti–6Al–4V alloys [16] indicate that the formation of a SiO_2 coating improves the oxidation resistance at 600 and 700 °C and also reduces the

S. K. Varma (✉) · C. Parga · K. Amato · J. Hernandez
Department of Metallurgical and Materials Engineering,
The University of Texas at El Paso, El Paso,
TX 79968-0520, USA
e-mail: skvarma@utep.edu

spallation and cracking of the oxide scales (consisting of Al_2O_3 and TiO_2). However, incorporation of Zr- and Hf-based oxides in the alumina scale for an FeCrAlY alloy [17] reduces the scale growth significantly during the oxidation in Ar–20O₂ at 1200 and 1300 °C. Fe–40Al prepared by elemental reaction synthesis [18] shows excellent oxidation resistance compared to pure Ti, Ni, and 316 stainless steels under cyclic oxidation conditions in air for 202 h at 600 and 800 °C. Presence of Mo in 316L stainless steel (SS) has shown [19] to possess better oxidation resistance than 304 SS by the formation of NiMoO_4 in the interior oxide–metal interface (by improving the adherence of the scale to the metal) when the oxidation was carried out at 900 °C in air. An interesting study presented by Ramanathan et al. [20] indicates that the addition of rare earth metals in the form of either elements or their oxides enhances the oxidation resistance of Fe–20Cr and Fe–20Cr–4Al alloy between 900 and 1100 °C. Apparently, the effect is more pronounced when the ionic radius of the rare earth metals is increased. Multilayer oxide scale has been shown [21] to develop in HfB_2 –20SiC between temperatures ranging from 1400 to 2000 °C under static and forced air conditions to simulate the atmospheric reentry. The layers are made up of SiO_2 in the outermost scale followed by HfO_2 and HfB_2 depleted in SiC. The lower viscosity of SiO_2 between 1800 and 1900 °C results in higher weight gain along with increase in the thickness of the scale.

Two ternary alloys from Nb–Cr–Si system appear to be providing a base for oxidation resistance alloy development [1, 6, 22]. The purpose of this paper is to report the results on a study to determine the oxidation resistance of two alloys from this system. The two alloys have different microconstituents, e.g., 20Cr alloy contains Nb_5Si_3 and Laves phase (NbCr_2) while 10Cr alloy contains $\text{Nb}_9\text{Si}_2\text{Cr}_3$ phase along with Nb_5Si_3 and NbCr_2 . The oxidation was carried out in stagnant air in a range of temperature from 700 to 1400 °C.

Experimental details

Nb–30Si–(10,20)Cr alloys (compositions are in atomic percents) were fabricated by the Ames Laboratory of Iowa State University using electric arc furnace under argon gas atmosphere. The $5 \times 5 \times 5$ mm samples were prepared by electric discharge machining (EDM) for use in oxidation experiments. This study uses the samples in the as-cast condition and a follow-up study, later, will consider the effect of annealed microstructures. Oxidation was carried out in air in a computer-controlled temperature furnace. Samples were heated at a rate of 10 °C/min, held at the oxidation temperature for 24 h and then furnace cooled (short term oxidation, STO). Oxidation

curves were plotted with weight gain per unit area as a function of temperature.

The characterization techniques included field emission electron microscope (FESEM), back scattered electron (BSE) imaging, X-ray mapping, energy dispersive spectroscopy (EDS). Hitachi S-4800 FESEM was used. X-ray diffraction (XRD) was performed in Bruker D6-Discover X-ray diffractometer (Table 1).

Results and discussion

Isothermal sections of Nb–Cr–Si phase diagrams were constructed using a Pandat™ software [23] from 700 to 1400 °C. The sections show that Nb–30Si–10Cr (10Cr alloy) alloy remains in a three phase region consisting of Laves phase (NbCr_2), 5–3 silicide (Nb_5Si_3), and $\text{Nb}_9\text{Si}_2\text{Cr}_3$ in the entire temperature range of this study. Nb–30Si–20Cr(20Cr alloy) is, however, a 2 phase alloy consisting of Laves phase and 5–3 silicide. Figure 1 shows the examples of two such isothermal sections at 700 and 1400 °C for illustration purpose. The as-cast microstructure of 10Cr alloy confirms the presence of three phases but 20Cr alloy also contains three phases as shown in Fig. 2. The three phases of 10Cr alloy are not in agreement with those predicted by the isothermal sections since the solid solution, α , is replaced by $\text{Nb}_9\text{Si}_2\text{Cr}_3$. The predicted two phases for 20Cr alloy, on the other hand, contains the additional $\text{Nb}_9\text{Si}_2\text{Cr}_3$ phase. This discrepancy may be attributed to the nonequilibrium processing conditions especially during casting.

Figure 3 shows the elemental distribution in the various phases for both alloys. Large concentrations of Nb and Si in the matrix shown by the maps for 20Cr alloy is indicative of the 3–5 silicide matrix while light gray areas clearly show the presence of Nb, Cr, and Si confirming the presence of $\text{Nb}_9\text{Si}_2\text{Cr}_3$. Laves phase is the dark phase in the microstructure. However, 10Cr alloy shows an example of the eutectic like microconstituent consisting of α , Laves phase, and 5–3 silicide. Again the 5–3 silicide matrix can be easily identified from these maps.

Short term oxidation (STO) curves for the two alloys are shown in Fig. 4, where weight gain per unit area as a function of oxidation temperature has been plotted. The oxidation resistance, based on the weight gain per unit area, appears to be better for 10Cr alloy at 800 °C but they are identical at 700 and 900 °C. It must be noted that both alloys show extensive pesting at 900, 1000, and 1100 °C and complete powder formation takes place for both alloys at the three temperatures. The 10Cr alloy, however, shows certain amount of metal still left in the crucible at 1000 °C. Higher temperature oxidation resistance (especially at 1200 and 1300 °C) for both alloys is remarkable even though 20Cr alloy shows better resistance. There is certain amount

Table 1 Summary of the oxidized products in both Nb–30Si–10Cr and Nb–30Si–20Cr alloys at various temperatures from 700 to 1400 °C

Temp °C	<i>o</i> -Nb ₂ O ₅ *	<i>m</i> -Nb ₂ O ₅ *	<i>β</i> -Nb ₂ O ₅ *	CrNbO ₄	SiO ₂	NbCr ₂	Nb ₅ Si ₃
700							
800							
900							
1000							
1100							
1200							
1300							
1400							

Source: Ref. [24]

of powder formation at 1400 °C for 10Cr alloy but the 20Cr alloy shows very little oxidation from 1200 to 1400 °C.

Oxide–metal interface (OMI) is shown in Fig. 5 for 10 and 20Cr alloys at 800 °C. Extensive porosity has been observed in the 20Cr alloy scale but the presence of CrNbO₄ and orthorhombic (*o*) form of Nb₂O₅ can be seen as dark and light gray phases, respectively. The structural forms of the oxides are based on the XRD results to be discussed later. The scale for 10Cr alloy, however, shows patches of unoxidized metal along with same two oxides that were observed for 20Cr alloy. The porosity levels, though, have been remarkably reduced for 10Cr alloy.

Oxide–metal interface (OMI) in the powdery region (from 900 to 1100 °C) appears only for 10Cr alloy at 1000 °C as shown in Fig. 6. Both alloys show complete disintegration into powder at 900 and 1100 °C but 10Cr alloy still contains OMI at 1000 °C while 20Cr alloy exhibits 100% pesting. Identification of oxides in the scale for 10Cr alloy at 1000 °C shows the presence of CrNbO₄ along with three forms (orthorhombic, *o*, monoclinic, *m*, and base centered monoclinic, *β*) of Nb₂O₅. Significance of this will be discussed later.

Figure 7 shows OMI for both alloys at 1200 °C. There are two striking features of the oxide identification in the scale for both alloys. First, SiO₂ begins to form at 1100 °C in these alloys as shown by the small black dots. Second, structural form of Nb₂O₅ changes from orthorhombic to monoclinic and no *β* form has been observed at temperatures above 1200 °C. However, there is still considerable amount of CrNbO₄ phase present in the scale for both alloys. Definite spalling can be noted for the 10Cr alloy in this figure. As noted earlier, this could be the result of large variations in the CTE values and the relative amounts of the oxides formed.

X-ray diffraction (XRD) results on the oxidized products appear to reveal considerable amount of information on the oxidation characteristics of the alloys. In the low temperature regime (700 and 800 °C), orthorhombic (*o*) form of Nb₂O₅ and CrNbO₄ have been confirmed while 10Cr alloy shows reflections for Laves and 3-5 silicide phases. But the powdery region developed at 900, 1000, and 1100 °C shows the presence of all three forms (*o*, *m*, *b*) of Nb₂O₅ plus the NbCrO₄ phases. High temperature oxidation, 1200, 1300, and 1400 °C, products clearly show the presence of only *m*-Nb₂O₅ and CrNbO₄ along with the

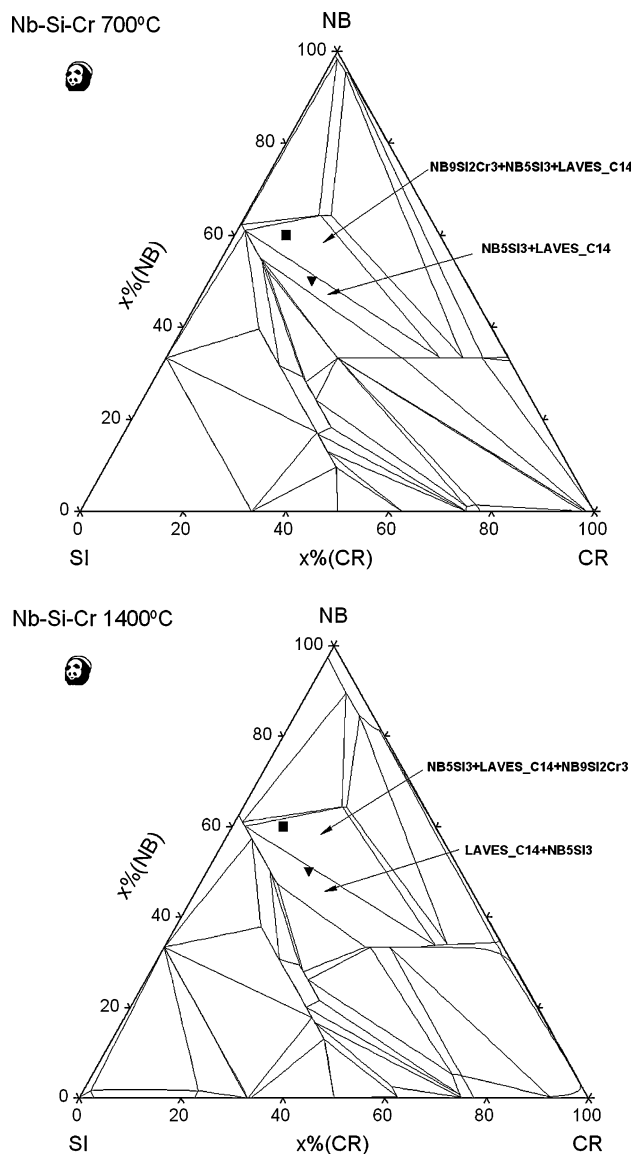


Fig. 1 Isothermal sections of Nb–Si–Cr phase diagram at 700 and 1400 °C as calculated by the Pandat™ software. The positions of Nb–30Si–10Cr and Nb–30Si–20Cr alloys have been marked. Even though only two sections have been shown, the phases predicted remain same for the entire temperature range from 700 to 1400 °C

formation of SiO_2 . Thus, it can be summarized that Nb_2O_5 undergoes polymorphic changes in both of these alloys while low and high temperature forms consists of orthorhombic and monoclinic, respectively. However, the formation of β - Nb_2O_5 takes place only in the intermediate temperature range corresponding to the powdery stage discussed earlier. The observation of three forms of Nb_2O_5 in their respective temperature ranges are in agreement with the results reported by Promisel [24]. It has been observed that the lattice expands twice when α - Nb_2O_5 transforms to β - Nb_2O_5 [25, 26]. Thus, it is possible to

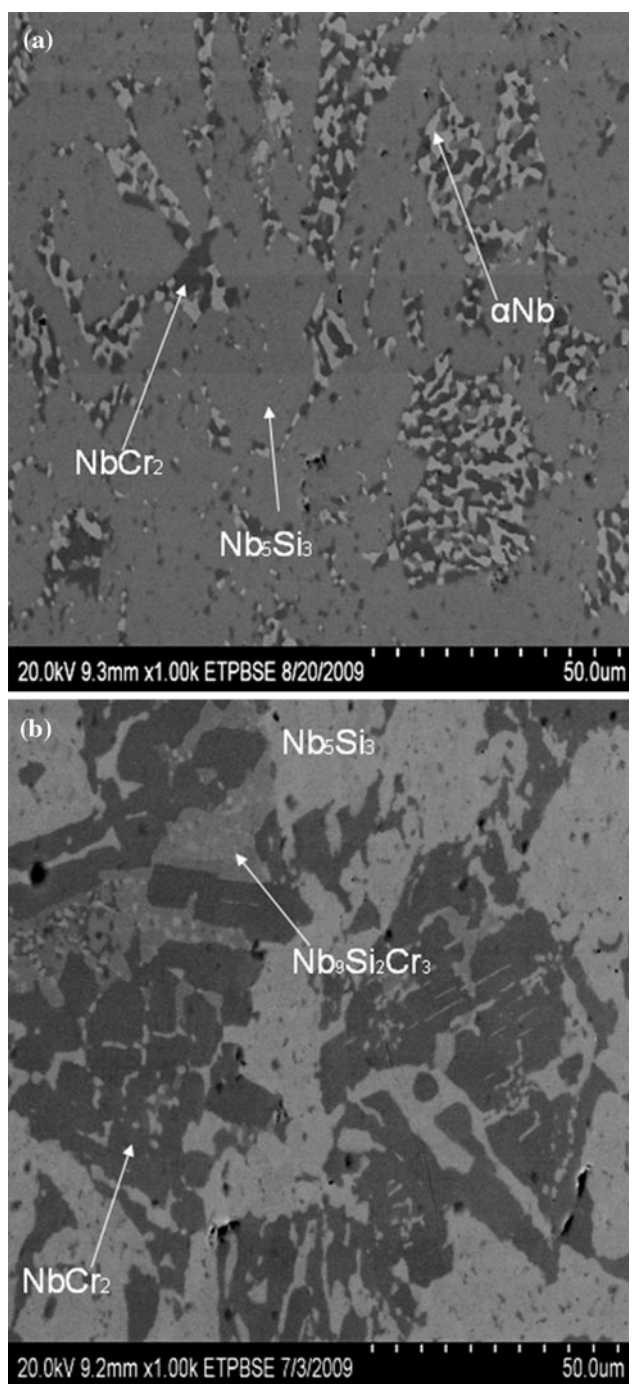


Fig. 2 As-cast microstructures of Nb–30Si–10Cr and Nb–30Si–20Cr alloys

conclude that the β - Nb_2O_5 formation is responsible for the extensive pesting observed at 900, 1000, and 1100 °C.

Conclusions

1. The observed microstructures for Nb–30Si–10Cr and Nb–30Si–20Cr alloys are not in agreement with the predicted phases by the Pandat™ software.

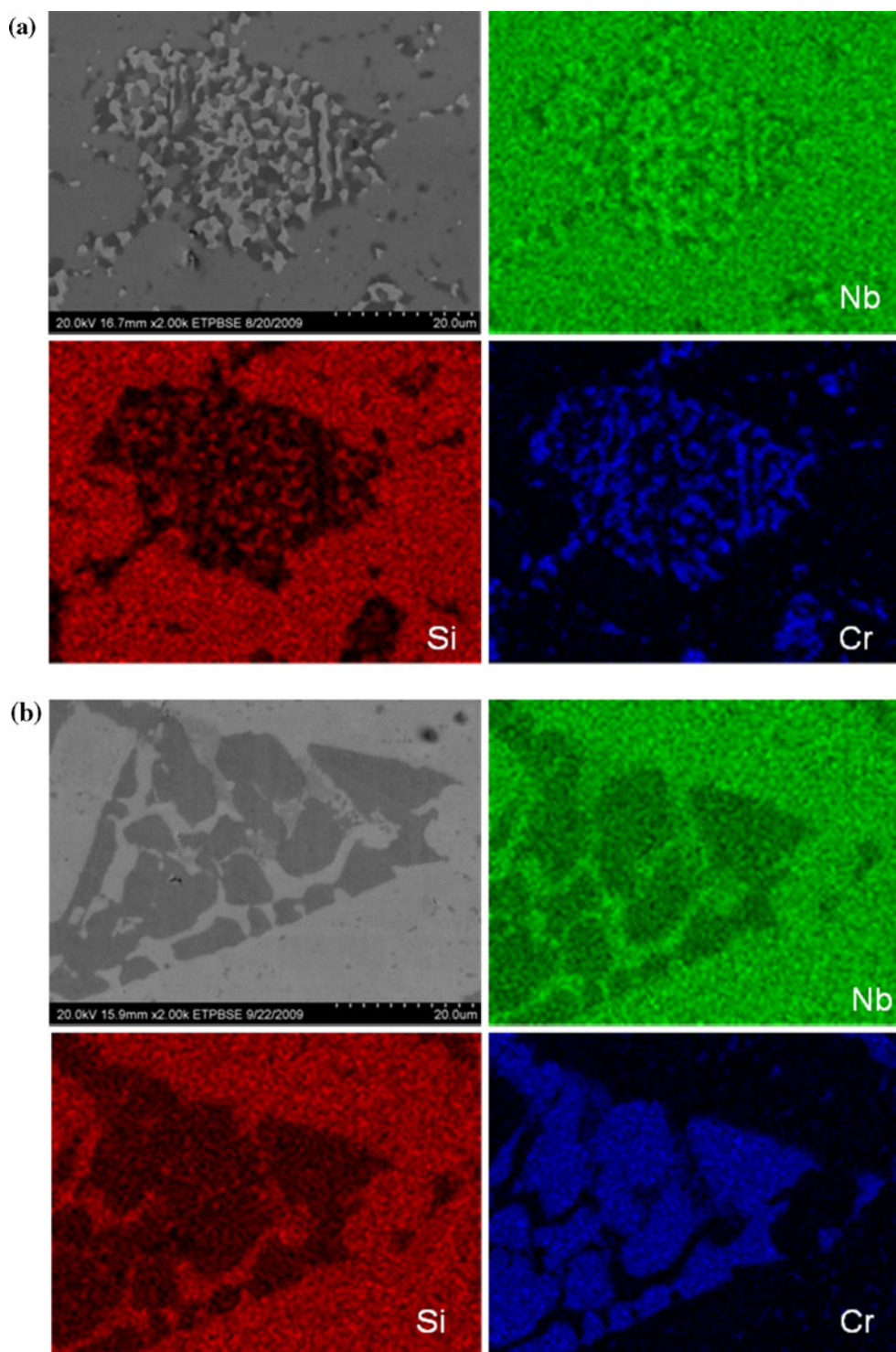


Fig. 3 X-ray mapping of **a** Nb–30Si–10Cr and **b** Nb–30Si–20Cr alloys showing elemental distributions in the various microconstituents

2. Extensive pesting occurs in these alloys at 900, 1000, and 1100 °C.
3. The two alloys show extremely good resistance from oxidation at high temperature. However, oxidation resistance of Nb–30Si–20Cr alloy is better than Nb–30Si–10Cr alloy at 1200, 1300, and 1400 °C.
4. The oxidation products in the scale have been found to be CrNbO_4 and various forms of Nb_2O_5 . Low

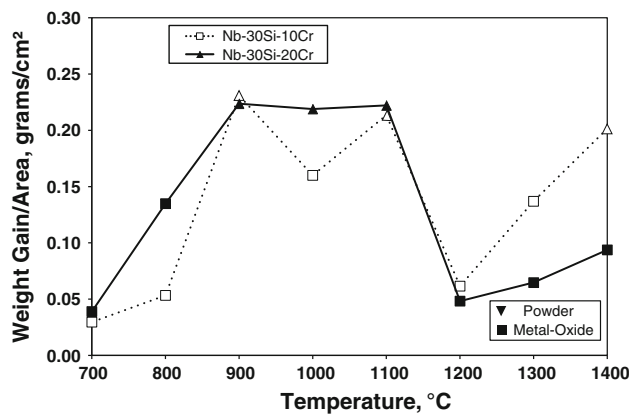


Fig. 4 Short term oxidation (STO) curves for Nb–30Si–10Cr and Nb–30Si–20Cr alloys from 700 to 1400 °C

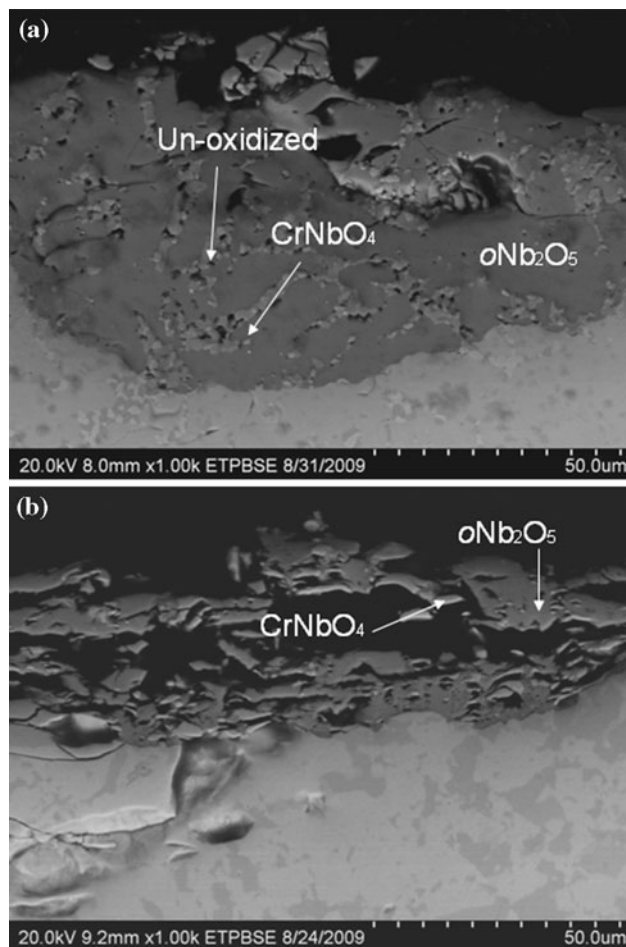


Fig. 5 Oxide–metal interface in Nb–30Si–10Cr and Nb–30Si–20Cr alloys oxidized at 800 °C

temperature form of Nb_2O_5 is orthorhombic while monoclinic structure develops at higher temperatures along with SiO_2 .

5. The enhanced oxidation resistance at 1200, 1300, and 1400 °C may be attributed to the formation of SiO_2 .

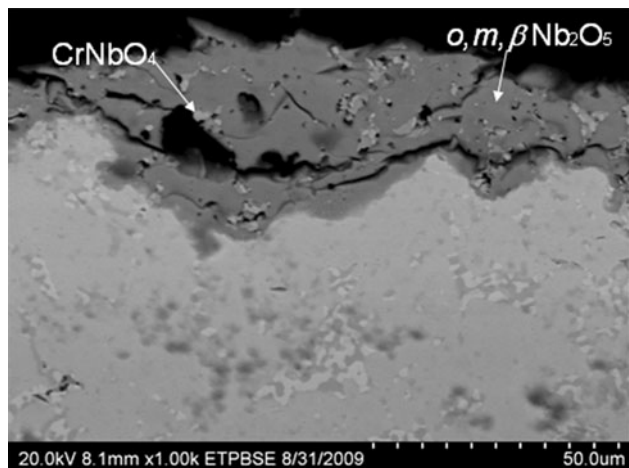


Fig. 6 Oxide–metal interface in Nb–30Si–10Cr alloy oxidized at 1000 °C

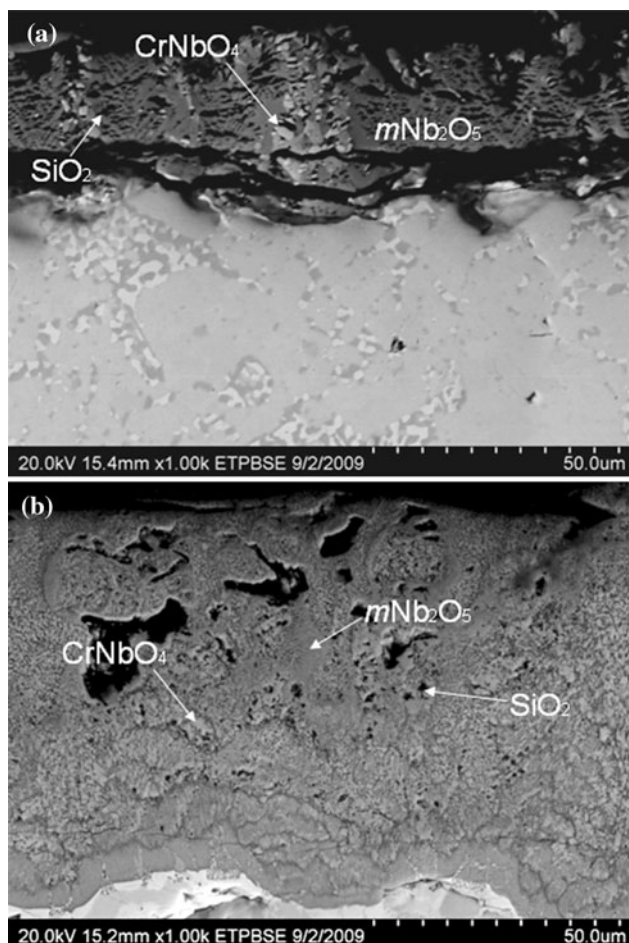


Fig. 7 Oxide–metal interface in Nb–30Si–10Cr and Nb–30Si–20Cr alloys oxidized at 1200 °C

6. Base centered monoclinic form, β , of Nb_2O_5 is primarily responsible for extensive peeling at 900, 1000, 1100 °C in the two alloys of this study.

Acknowledgements The authors wish to acknowledge the financial support of Office Naval Research (ONR) through the grant number N00014-08-1-0506. Dr. David Shifler is the program manager.

References

1. Natividad S, Acosta A, Amato K, Ventura J, Portillo B, Varma SK (2010) Mater Sci Forum 638–642:2351
2. Moricca M, Varma SK (2010) J Alloys Compd 490:195
3. Portillo B, Kakarlapudi P, Varma SK (2007) J Met 59(6):46
4. Moricca M, Varma SK (2008) J Met 60(7):66
5. Ventura J, Portillo B, Varma SK (2009) J Alloys Compd 476:257
6. Ventura J, Varma SK (2009) J Met 61(7):72
7. Ventura J, Portillo B, Varma SK, Mahapatra RN (2009) ECS Trans 16(44):157
8. Chan KS (2004) Oxid Met 61(3–4):165
9. Chan KS (2004) Metall Mater Trans A 35A:589
10. Bewlay B, Jackson M, Lipsitt H (1996) Metall Mater Trans A 27A:3801
11. Bewlay BP, Dovideenko K, Ellis KD, Deal A, Cournoyer J (2006) Microstruct Microanal 12 (supp 2). doi:[10.101/S1431927606068723](https://doi.org/10.101/S1431927606068723)
12. Zheng H, Lu S, Jianye Z, Guangming L (2009) Int J Refract Metal Hard Mater 27:659
13. Bewlay BP, Jackson MR, Gigliotti MFX (2002) In: Westbrook JH, Fleisher RL (eds) Intermetallic compounds, principles and practice, vol 3. Wiley, New York, USA
14. Bewlay BP, Jackson MR, Zhao J-C, Subramanian PR (2003) Metall Mater Trans A 34A:2043
15. Geng J, Tsakirooulos P, Shao G (2006) Mater Sci Eng A 441:26
16. Zang XJ, Gao YH, Ren BY, Tsubaki N (2010) J Mater Sci 45:1622. doi:[10.1007/s10853-009-4138-8](https://doi.org/10.1007/s10853-009-4138-8)
17. Naumenko D, Kochubey V, Niewolak L, Dymati A, Mayer J, Singheiser L, Quadakkers (2008) J Mater Sci 43:4550. doi:[10.1007/s10853-008-2639-5](https://doi.org/10.1007/s10853-008-2639-5)
18. Shen PZ, Song M, Gao HY, He YH, Zou J, Xu NP, Huang BY, Liu YH (2009) J Mater Sci 44:4413. doi:[10.1007/s10853-009-3669-3](https://doi.org/10.1007/s10853-009-3669-3)
19. Buscail H, Messki SE, Riffard F, Perrier S, Cueff R, Issartel (2008) J Mater Sci 43:6960. doi:[10.1007/s10853-008-2965-7](https://doi.org/10.1007/s10853-008-2965-7)
20. Ramanathan LV, Pillis MF, Fernandez SMC (2008) J Mater Sci 43:530. doi:[10.1007/s10853-007-1855-8](https://doi.org/10.1007/s10853-007-1855-8)
21. Carney CM (2009) J Mater Sci 44:5673. doi:[10.1007/s10853-009-3799-7](https://doi.org/10.1007/s10853-009-3799-7)
22. Murakami MR, Sasaki S, Ichikawa K, Kitahara A (2001) Intermetallics 9:629
23. PANDATTM (2007) Phase diagram calculation software for multicomponent systems. Computherm LLC, Madison, WI 53719
24. Promisel NE (1963) In: Conference on refractory metals at Oslo University Centre, Oslo-Blindern, Norway. Tungsten, tantalum, molybdenum, niobium and their alloys, June 23–26. Pergamon Press, NY, USA, pp 295–329
25. Arbuzev MP, Chupria VG (1963) Institute of cermets and special alloys, September. pp 87–89
26. Ercit TS (1991) Mineral Petrol 43:217